A trigonometric interpolation approach to mixed-type boundary problems associated with permeameter shape factors

Harald Klammler,[1,2,3] Kirk Hatfield,[1,2] Bassel Nemer,[1,2] and Simon A. Mathias[4]

Received 18 March 2010; revised 1 November 2010; accepted 12 January 2011; published 8 March 2011.

[1] Hydraulic conductivity is a fundamental hydrogeological parameter, whose in situ measurement at a local scale is principally performed through injection tests from screened probes or using impermeable packers in screened wells. The shape factor F [L] is a proportionality constant required to estimate conductivity from observed flow rate to injection head ratios, and it depends on the geometric properties of the flow field. Existing approaches for determination of F are either based on geometric or mathematical simplifications and are limited to particular assumptions about the flow domain's external boundaries. The present work presents a general semianalytical solution to steady state axisymmetric flow problems, where external boundaries may be nearby and of arbitrary combinations of impermeable and constant head type. The inner boundary along the probe or well may consist of an arbitrary number of impermeable and constant head intervals resulting in a mixed-type boundary value problem, for which a novel and direct solution method based on trigonometric interpolation is presented. The approach is applied to generate practical nondimensional charts of F for different field and laboratory situations. Results show that F is affected by less than 5% if a minimum distance of 10 probe or well diameters is kept between the injection screen and a nearby boundary. Similarly, minimum packer lengths of two well diameters are required to avoid increasing F by more than 10%. Furthermore, F is determined for laboratory barrel experiments giving guidelines for achieving equal shape factors as in field situations without nearby boundaries. F for the theoretical case of infinitely short packers is shown to be infinitely large.

Citation: Klammler, H., K. Hatfield, B. Nemer, and S. A. Mathias (2011), A trigonometric interpolation approach to mixed-type boundary problems associated with permeameter shape factors, *Water Resour. Res., 47*, W03510, doi:10.1029/2010WR009337.

1. Introduction

[2] Hydraulic conductivity K [L/T] with its horizontal and vertical variability is a parameter of paramount importance for the modeling and management of a large number of natural and engineered processes, including infiltration, irrigation, drainage, groundwater extraction and injection, soil compaction, landfill impermeabilization, and contaminant transport [*Sedighi et al.*, 2006; *Sudicky*, 1986; *Hvorslev*, 1951]. Under saturated conditions, i.e., below the water table of an aquifer, classically, pump or slug tests with their well-known individual advantages and drawbacks are performed for investigations of K at different scales [*Weight and Sonderegger*, 2001]. Accordingly, these tests may be performed on an entire well or on various portions of a well screen by use of single- or double-packer systems [*Butler et al.*, 2009; *Price and Williams*, 1993]. Different types of small-diameter (i.e., lower centimeter range) drive point (also called push-in or direct-push) probes have also been proposed for quick and flexible investigation of K in unconsolidated media at highly local (i.e., <1 m^3) scales. Because of the small spatial scale the associated flow systems reach steady state rapidly and do not require a permanent installation of an injection well or piezometers around it. Using such push-in probes with short injection screen intervals near the probe tips, *Hinsby et al.* [1992] demonstrate a "mini slug test" method, while *Butler et al.* [2007] and *Dietrich et al.* [2008] apply a "direct-push permeameter" and a "direct-push injection logger," respectively. The difference between the latter two direct-push methods is that the injection logger uses the variability in recorded ratios of injection pressures and flow rates as a function of depth to estimate variability in local K without, however, assigning absolute K values. The "push-in permeameter" uses two additional head observations along the probe to also quantify absolute values of K. Whenever the goal is to estimate such absolute values of K, a so-called shape factor (often denoted by F [L]) is required, which serves as the proportionality constant between ratios of observed injection flow rates Q [L^3/T] to injection heads ϕ_0 [L] and K. Thus, knowing F and observing Q/ϕ_0, K can be estimated from

[1]Department of Civil and Coastal Engineering, University of Florida, Gainesville, Florida, USA.
[2]Interdisciplinary Program in Hydrologic Sciences, University of Florida, Gainesville, Florida, USA.
[3]Department of Environmental Sciences and Sustainable Development, Federal University of Bahia, Barreiras, Brazil.
[4]Department of Earth Sciences, Durham University, Durham, UK.

0043-1397/11/2010WR009337

$$K = \frac{Q}{\phi_0 F} \tag{1}$$

[3] More precisely, ϕ_0 hereby is the excess hydraulic head at the screen because of pumping with respect to ambient (no pumping) conditions, and as used in the sequel, it is assumed to be constant both in time (steady state) as well as over the injection screen surface.

[4] Many variants of in situ measurement methods for K have been developed, and a correspondingly large number of theoretical models have been invoked for test interpretation, i.e., determination of F. However, a common feature of virtually all methods is that an axially (or rotationally) symmetric potential flow field is generated through injection or extraction of water from some cylindrical well or probe surface, which may or may not include the tip of a well or probe. An important and complicated issue is the presence of mixed-type boundary conditions, which arises because of the simultaneous presence of both no-flow and constant head segments along the inner boundary associated with the well or probe surface.

[5] Early models which persist until the present day apply geometric approximations of the cylindrical (constant head) injection surface by spheroids [*Mathias and Butler*, 2006; *Hvorslev*, 1951]. Other approximations use distributed point sources along a line [*Zlotnik and Ledder*, 1996] or over a cylindrical surface [*Peursem et al.*, 1999]. More recently, computationally intensive finite difference or finite element methods have been used to better reproduce geometric and hydraulic boundary conditions at the injection screen [*Liu et al.*, 2008; *Ratnam et al.*, 2001]. Another approach that has proved popular involves conversion of the mixed-type boundary problem along the well or probe into a single-type boundary problem by either assuming approximate flux distributions along constant head boundary segments [*Chang and Chen*, 2002, 2003; *Rehbinder*, 2005; *Perina and Lee*, 2006; *Mathias and Butler*, 2007] or assuming approximate head distributions along no flow boundary segments [*Rehbinder*, 1996]. While the analytical approaches of *Rehbinder* [1996, 2005] use predefined continuous functions for these approximations, *Chang and Chen* [2002, 2003], *Perina and Lee* [2006], and *Mathias and Butler* [2007] use adjustable functions by making them piecewise constant in a semianalytical approach.

[6] In what follows we take advantage of a general solution given by *Zaslavsky and Kirkham* [1964] to derive different forms of steady state solutions to the axisymmetric flow problem for all possible combinations of constant head and impermeable top, bottom, and lateral boundaries at arbitrary distances. We further present a novel, direct, and simple semianalytical method related to trigonometric interpolation to directly deal with the mixed boundary value problem along the injection well or probe (i.e., without requiring conversion into a single-type boundary value problem as done in previous work) and use the observed convergence behavior to extrapolate toward exact solutions. Results are applied to investigate effects of nearby boundaries on injection test results and to provide practical charts of shape factors F for different scenarios. Validation is achieved by comparison with equivalent results previously obtained by *Mathias and Butler* [2007] for sufficiently distant boundaries such that they can be ignored. A clarification is also made concerning the divergent series contained within *Mathias and Butler*'s [2007] previous analytical solution for infinitesimally short packers.

[7] Although injection tests from push-in probes or packered-off screen intervals may be limited to local scales not containing any external boundaries, situations may arise where proximity to a confining layer, a surface water body, or the water table has to be accounted for [*Lui et al.*, 2008]. In particular, injection near constant head boundaries may be strongly distorted because of flow short-circuiting between the screen and the boundary. Similarly, laboratory testing in sand barrels is a routine procedure for injection test calibration, and the effects of nearby impermeable barrel walls deserve particular investigation.

2. General Solution of the Flow Problem

[8] An example of an axisymmetric flow domain is given in Figure 1, where r [L] and z [L] are the radial and vertical coordinates, respectively, being delimited by $a < r < b$ [L] and $0 < z < d$ [L]. To represent the radius of the probe or well, a is used, which is assumed to span the entire distance d between top and bottom boundaries, while b is the radial distance to a lateral boundary. Moreover, h_1 through h_4 [L] delimit different boundary type segments along the well or probe. The governing Laplace equation for steady state flow and isotropic hydraulic conductivity in axisymmetric cylindrical coordinates is

$$\frac{\partial^2 \phi}{\partial r^2} + \frac{1}{r}\frac{\partial \phi}{\partial r} + \frac{\partial^2 \phi}{\partial z^2} = 0, \tag{2}$$

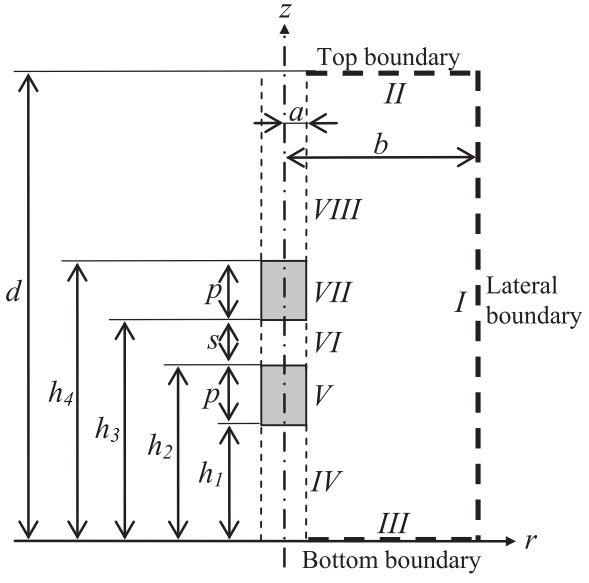

Figure 1. Example of axisymmetric flow domain with double-packer injection from a fully screened well and nearby boundaries. I, constant head or impermeable lateral boundary; II, constant head or impermeable top; III, constant head or impermeable bottom; IV and VIII, constant head open well screen intervals; V and VII, impermeable packers; VI, constant head injection screen interval. The flow domain is delimited by two coaxial cylinders between $0 < z < d$ and $a < r < b$. For injection from a push-in probe, boundaries IV and VIII are impermeable as well (i.e., $h_1 = 0$ and $h_4 = d$).

where $\phi = \phi(r, z)$ [L] is the hydraulic head distribution in the flow domain. A general solution of equation (2) is given by *Zaslavsky and Kirkham* [1964] as

$$\begin{aligned}\phi(r,z) = {} & [c_1 \sin(m_1 z) + c_2 \cos(m_1 z)][c_3 \mathrm{I}_0(m_1 r) + c_4 \mathrm{K}_0(m_1 r)] \\ & + [c_5 \sinh(m_2 z) + c_6 \cosh(m_2 z)][c_7 \mathrm{J}_0(m_2 r) + c_8 \mathrm{Y}_0(m_2 r)] \\ & + c_9 z \ln(r/m_3) + c_{10} \ln(r/m_3) + c_{11} z + c_{12},\end{aligned} \tag{3}$$

where c_i for $i = 1, 2, \ldots, 12$ and m_i for $i = 1, 2, 3$ are arbitrary real constants (m_i being positive) and I_0, K_0, J_0, and Y_0 are Bessel functions of order zero [*Dwight*, 1947]. By superimposing solutions of equation (3) with different sets of constants, specific boundary conditions, including arrangements of mixed-type boundary conditions (this becomes clearer in the subsequent discussion), can be met. This will first be done for external boundaries I, II, and III shown in Figure 1 and subsequently for internal boundary segments IV–VIII along the well or probe.

2.1. External Boundaries

[9] While the types of internal boundary conditions along the probe are defined by the injection test setup, the types of external boundaries may be different combinations of constant head and impermeable. Both top and bottom boundaries may be considered impermeable, for example, if an injection test is performed in a (thin) stratum between two confining layers. In the case of permeability injection testing of a sealing layer under a landfill, for example, both top and bottom boundaries may be well approximated by two constant head boundaries. A mix of constant head top and impermeable bottom boundary may well represent conditions in a (shallow) unconfined aquifer or beneath surface water bodies. If the distance between injection screen and one or both of top and bottom boundaries is sufficiently small, an impact of the nearby boundary (boundaries) onto the outcome of the injection test may be expected and accounted for by a respective adjustment in the shape factor F. Similarly, modeling an impermeable lateral boundary is of interest for laboratory barrel tests, where either top, bottom, or both boundaries are constant head, while the lateral barrel wall is impermeable. Thus, the external boundary conditions in Figure 1 may be represented as follows: I, constant head ($\mathrm{I_c}$) or impermeable ($\mathrm{I_i}$) lateral boundary; II, constant head ($\mathrm{II_c}$) or impermeable ($\mathrm{II_i}$) top boundary; III, constant head ($\mathrm{III_c}$) or impermeable ($\mathrm{III_i}$) bottom boundary. Mathematically, this can be expressed as

$$\mathrm{I_c} \quad \phi = 0 \quad \text{at} \quad r = b \quad \text{for} \quad 0 \le z \le d, \tag{4a}$$

$$\mathrm{I_i} \quad \frac{\partial \phi}{\partial r} = 0 \quad \text{at} \quad r = b \quad \text{for} \quad 0 \le z \le d, \tag{4b}$$

$$\mathrm{II_c} \quad \phi = 0 \quad \text{at} \quad z = d \quad \text{for} \quad a \le r \le b, \tag{5a}$$

$$\mathrm{II_i} \quad \frac{\partial \phi}{\partial z} = 0 \quad \text{at} \quad z = d \quad \text{for} \quad a \le r \le b, \tag{5b}$$

$$\mathrm{III_c} \quad \phi = 0 \quad \text{at} \quad z = 0 \quad \text{for} \quad a \le r \le b, \tag{6a}$$

$$\mathrm{III_i} \quad \frac{\partial \phi}{\partial z} = 0 \quad \text{at} \quad z = 0 \quad \text{for} \quad a \le r \le b. \tag{6b}$$

[10] Using extensions of *Kirkham* [1959] and *Boast and Kirkham* [1971], solutions in terms of the hydraulic head ϕ, which honor equations (4), (5) and (6) under all possible scenarios of boundary type combinations, may be based on the following considerations and written as follows.

[11] 1. Considering constant head top and bottom boundaries, i.e., $\phi(z = 0) = \phi(z = d) = 0$ for all $a \le r \le b$, of all the terms in z in equation (3), these conditions can be met by $\sin(m_1 z)$ with $m_1 = n\pi / d$ as well as n and N being arbitrary positive integers, such that after superposition

$$\phi(r,z) = \sum_{n=1}^{N} B_n f_0(m_1 r) \sin(m_1 z), \; m_1 = n\pi / d\,. \tag{7}$$

[12] B_n are a new set of constants encompassing c_1, c_3, and c_4, and $f_0(m_1 r)$ is a function to be defined involving terms of equation (3) containing $K_0(m_1 r)$ and $I_0(m_1 r)$.

[13] 2. Considering impermeable top and bottom boundaries, i.e., $\partial\phi / \partial z = 0$ at $z = 0$ and $z = d$ for all $a \le r \le b$, of the terms in z in equation (3), these conditions can be met by $\cos(m_1 z)$ with $m_1 = n\pi / d$ as well as by $\ln(r/m_3)$ with arbitrary m_3 and by the final (arbitrary) constant, which may be incorporated into m_3. Superposition of these solutions gives

$$\phi(r,z) = B_0 \frac{\ln(b/r)}{\ln(b/a)} + \sum_{n=1}^{N} B_n f_0(m_1 r) \cos(m_1 z), \; m_1 = n\pi / d\,. \tag{8}$$

[14] B_n and f_0 are analogous to equation (7), and B_0 is an additional constant; $c_{12} = 0$ and $m_3 = b$ are chosen such that the leading term on the right-hand side becomes zero for $r = b$, as required for a constant zero head boundary at radial distance b. The constant term $\ln(b/a)$ in the denominator is added to simplify expressions in the sequel by taking the ratio to 1 for $r = a$ and allowing for a particular interpretation of B_0.

[15] 3. Considering impermeable top and constant head bottom boundary, i.e., $\phi(z = 0) = 0$ and $\partial\phi / \partial z = 0$ at $z = d$ for all $a \le r \le b$, of the terms in z in equation (3), the first (constant head) condition may be met by $\sin(m_1 z)$, $\sinh(m_2 z)$, $z\ln(r/m_3)$, and z, where m_1, m_2, and m_3 may be arbitrary. Among these solutions, however, the second (no flow) condition may only be satisfied by $\sin(m_1 z)$ with $m_1 = (2n - 1)\pi / (2d)$ such that superposition leads to

$$\phi(r,z) = \sum_{n=1}^{N} B_n f_0(m_1 r) \sin(m_1 z), \; m_1 = (2n - 1)\pi/(2d)\,. \tag{9}$$

[16] It is observed that equations (7), (8), and (9) meet boundary conditions II and III independent of the choice of the coefficients B_0 and B_n and the function f_0. This allows using f_0 to independently satisfy the type of lateral boundary condition I in equations (7), (8), and (9). From equation (3) and its terms in z retained in equations (7), (8), and (9), it is evident that f_0 has to consist of linear combinations of $K_0(m_1 r)$ and $I_0(m_1 r)$ as follows.

[17] 1. For constant head lateral boundary, i.e., $\phi = 0$ at $r = b$ for all $0 \le z \le d$, this can be achieved by imposing $c_3 I_0(m_1 b) + c_4 K_0(m_1 b) = 0$ in equation (3) and results in

$$f_{0c}(m_1 r) = \frac{\frac{K_0(m_1 r)}{K_0(m_1 b)} - \frac{I_0(m_1 r)}{I_0(m_1 b)}}{\frac{K_0(m_1 a)}{K_0(m_1 b)} - \frac{I_0(m_1 a)}{I_0(m_1 b)}} \approx \frac{K_0(m_1 r)}{K_0(m_1 a)}, \tag{10}$$

where additional constants are included to make $f_{0c} = 1$ at $r = a$ for later convenience. For later convenience and knowing that $dK_0(r)/dr = -K_1(r)$ and $dI_0(r)/dr = I_1(r)$, we also introduce

$$f_{1c}(m_1 r) = -\frac{1}{m_1}\frac{df_{0c}}{dr} = \frac{\frac{K_1(m_1 r)}{K_0(m_1 b)} + \frac{I_1(m_1 r)}{I_0(m_1 b)}}{\frac{K_0(m_1 a)}{K_0(m_1 b)} - \frac{I_0(m_1 a)}{I_0(m_1 b)}} \approx \frac{K_1(m_1 r)}{K_0(m_1 a)}. \tag{11}$$

[18] 2. For impermeable lateral boundary, i.e., $\partial\phi/\partial r = 0$ at $r = b$ for all $0 \le z \le d$, this condition may be achieved by assuring $f_{1i} = -(1/m_1)df_{0i}/dr = 0$ for $r = b$ in equations (7) and (9). Since f_{0i} has to be a linear combination of I_0 and K_0 and because of the respective derivatives given above, f_{1i} has to be a linear combination of I_1 and K_1, such that imposing $c_3 I_1(m_1 b) + c_4 K_1(m_1 b) = 0$ leads to

$$f_{1i}(m_1 r) = -\frac{1}{m_1}\frac{df_{0i}}{dr} = \frac{\frac{K_1(m_1 r)}{K_1(m_1 b)} - \frac{I_1(m_1 r)}{I_1(m_1 b)}}{\frac{K_1(m_1 a)}{K_1(m_1 b)} - \frac{I_1(m_1 a)}{I_1(m_1 b)}} \approx \frac{K_1(m_1 r)}{K_1(m_1 a)}, \tag{12}$$

where additional constants are used to make $f_{1i} = 1$ for $r = a$. From this, f_{0i} may be obtained by integration as

$$f_{0i}(m_1 r) = \frac{\frac{K_0(m_1 r)}{K_1(m_1 b)} + \frac{I_0(m_1 r)}{I_1(m_1 b)}}{\frac{K_1(m_1 a)}{K_1(m_1 b)} - \frac{I_1(m_1 a)}{I_1(m_1 b)}} \approx \frac{K_0(m_1 r)}{K_1(m_1 a)}. \tag{13}$$

[19] In the case of equation (8), where top and bottom are already impermeable, an impermeable lateral boundary only makes physical sense if the same flow injected is again extracted by the well or probe (e.g., vertical recirculation well [*Zlotnik and Ledder*, 1996; *Peursem et al.*, 1999]). If this is the case, then it can be shown that $B_0 = 0$, and hence, $\partial\phi/\partial r = 0$ for $r = b$ is again met. The approximations given with equations (10)–(13) are for large values of b/a and become exact for $b \to \infty$, i.e., laterally unbounded flow domains (both $K_0(m_1 b)$ and $K_1(m_1 b)$ approach zero in this case, while both $I_0(m_1 b)$ and $I_1(m_1 b)$ approach infinity).

2.2. Trigonometric Interpolation Approach to the Mixed-Type Internal Boundaries

[20] In equations (7), (8), and (9), the values of the coefficients B_0 and B_n do not affect compliance with the external boundary conditions I, II, and III such that these coefficients can be used to independently meet the internal (mixed) boundary conditions along the device (i.e., for $r = a$). According to Figure 1, for a double-packer test these boundaries are constant head open screen interval at bottom (IV), impermeable bottom packer (V), constant head injection screen interval (VI), impermeable top packer (VII), and constant head open screen interval at top (VIII). Mathematically, this may be written as

$$\text{IV} \quad \phi = \phi_{\text{IV}} \quad \text{at} \quad r = a \quad \text{for} \quad 0 \le z \le h_1, \tag{14}$$

$$\text{V} \quad \frac{\partial\phi}{\partial r} = 0 \quad \text{at} \quad r = a \quad \text{for} \quad h_1 \le z \le h_2, \tag{15}$$

$$\text{VI} \quad \phi = \phi_0 \quad \text{at} \quad r = a \quad \text{for} \quad h_2 \le z \le h_3, \tag{16}$$

$$\text{VII} \quad \frac{\partial\phi}{\partial r} = 0 \quad \text{at} \quad r = a \quad \text{for} \quad h_3 \le z \le h_4, \tag{17}$$

$$\text{VIII} \quad \phi = \phi_{\text{VIII}} \quad \text{at} \quad r = a \quad \text{for} \quad h_4 \le z \le d, \tag{18}$$

where ϕ_{IV} and ϕ_{VIII} [L] are the constant hydraulic heads in the bottom and top open screen intervals, respectively. In order to determine B_0 and B_n, the respective "raw" solution of $\phi(r, z)$ for a given set of external boundary conditions from equations (7), (8), or (9) is substituted into equations (14)–(18). Considering, for example, the case of impermeable top and bottom boundaries in combination with a constant head lateral boundary, equation (8) (with $f_0 = f_{0c}$ and f_{1c} from equations (10) and (11)) is used to obtain the following system of equations to impose the internal boundary conditions.

$$\phi(a,z) = B_0 + \sum_{n=1}^{N} B_n \cos(m_1 z) = \phi_{\text{IV}}, \quad 0 \le z \le h_1, \tag{19}$$

$$-\left.\frac{\partial\phi}{\partial r}\right|_{r=a} = \frac{B_0}{a\ln(b/a)} + \sum_{n=1}^{N} B_n \frac{n\pi}{d} f_{1c}(m_1 a)\cos(m_1 z) = 0, \quad h_1 \le z \le h_2, \tag{20}$$

$$\phi(a,z) = B_0 + \sum_{n=1}^{N} B_n \cos(m_1 z) = \phi_0, \quad h_2 \le z \le h_3, \tag{21}$$

$$-\left.\frac{\partial\phi}{\partial r}\right|_{r=a} = \frac{B_0}{a\ln(b/a)} + \sum_{n=1}^{N} B_n \frac{n\pi}{d} f_{1c}(m_1 a)\cos(m_1 z) = 0, \quad h_3 \le z \le h_4, \tag{22}$$

$$\phi(a,z) = B_0 + \sum_{n=1}^{N} B_n \cos(m_1 z) = \phi_{\text{VIII}}, \quad h_4 \le z \le d. \tag{23}$$

[21] To achieve an exact solution, N must be set to infinity, for which equations (7), (8), and (9) become Fourier series. Although *Sneddon* [1966] discusses solutions to similar systems of equations, analytical solutions for the mixed-type boundary value problems are generally intractable.

[22] However, by limiting N to finite values (i.e., truncating the trigonometric series) and discretizing the device length $0 \le z \le d$ into a number N_B (dimensionless) of equidistant intervals delimited by z_{i-} and z_{i+} with $i = 1, 2, \ldots, N_B$, such that $z_{1-} = 0$, $z_{NB+} = d$, $z_{i+} = z_{(i+1)-}$, $z_{i+} - z_{i-} = d/N_B$, and $z_i = (z_{i+} + z_{i-})/2$, equations (19)–(23) may be

rewritten in a discretized form by simply substituting z_i for z everywhere. With this, equations (19)–(23) constitute a linear system of N_B equations in $N+1$ unknown coefficients. This system may be regarded in a curve-fitting context, where it is the goal to determine the unknown coefficients of equation (8) (for finite N) to best approximate the right-hand sides of equations (19)–(23) containing punctual information about ϕ and $\partial\phi/\partial r$. For $N_B > N+1$, this may be done in a linear regression (i.e., least squares) sense, while for $N_B = N+1$, curve fitting becomes exact and thus transitions into the field of trigonometric interpolation. For $N_B < N+1$, the system is underdetermined. In the present work, N_B is set equal to the number of unknown coefficients, i.e., $N+1$ or N, depending on whether B_0 is present or not. Note that the discretized well flux approach presented previously by *Mathias and Butler* [2007] represents a special case of the more general approach presented above.

[23] Before solving the resulting system it is noted that ϕ_{IV} and/or ϕ_{VIII} in equations (19)–(23) are only known if the top and bottom open screen intervals are connected to constant head top and/or bottom boundaries. For impermeable top and bottom boundaries, ϕ_{IV} and ϕ_{VIII} are initially unknown, but instead, two additional equations can be formulated imposing zero total (i.e., integrated over z) inflows or outflows Q_{IV} and Q_{VIII} [L^3/T] from the open screen intervals below and above the packers, respectively:

$$\frac{Q_{\mathrm{IV}}}{2\pi aK} = -\int_0^{h_1} \left.\frac{\partial\phi}{\partial r}\right|_{r=a} \mathrm{d}z = \frac{B_0 h_1}{a\ln\frac{b}{a}} + \sum_{n=1}^{N} B_n f_{1c}(m_1 a)\sin(m_1 h_1) = 0, \tag{24}$$

$$\frac{Q_{\mathrm{VIII}}}{2\pi aK} = -\int_{h_4}^{d} \left.\frac{\partial\phi}{\partial r}\right|_{r=a} \mathrm{d}z = \frac{B_0(d-h_4)}{a\ln\frac{b}{a}} - \sum_{n=1}^{N} B_n f_{1c}(m_1 a)\sin(m_1 h_4) = 0. \tag{25}$$

[24] The result is an extended system of N_B+2 linear equations in N_B+2 unknowns, for which many standard methods are available for the solution. For example, equations (19)–(25) may be converted from summation into matrix form $[\mathbf{A}]\times[\mathbf{B}] = [\mathbf{C}]$, giving

$$\begin{bmatrix}
1 & \cos(\pi z_1/d) & \cos(2\pi z_1/d) & \cdots & \cos(Nz_1/d) & -1 & 0 \\
\vdots & \vdots & \vdots & \vdots & \vdots & \vdots & \vdots \\
1 & \cos(\pi z_{N_{\mathrm{IV}}}/d) & \cos(2\pi z_{N_{\mathrm{IV}}}/d) & \cdots & \cos(Nz_{N_{\mathrm{IV}}}/d) & -1 & 0 \\
\frac{1}{a\ln(b/a)} & \frac{\pi}{d}f_{1c}(\frac{\pi a}{d})\cos(\frac{\pi z_{N_{\mathrm{IV}}+1}}{d}) & \frac{2\pi}{d}f_{1c}(\frac{2\pi a}{d})\cos(\frac{2\pi z_{N_{\mathrm{IV}}+1}}{d}) & \cdots & \frac{N\pi}{d}f_{1c}(\frac{N\pi a}{d})\cos(\frac{N\pi z_{N_{\mathrm{IV}}+1}}{d}) & 0 & 0 \\
\vdots & \vdots & \vdots & \vdots & \vdots & \vdots & \vdots \\
\frac{1}{a\ln(b/a)} & \frac{\pi}{d}f_{1c}(\frac{\pi a}{d})\cos(\frac{\pi z_{N_{\mathrm{V}}}}{d}) & \frac{2\pi}{d}f_{1c}(\frac{2\pi a}{d})\cos(\frac{2\pi z_{N_{\mathrm{V}}}}{d}) & \cdots & \frac{N\pi}{d}f_{1c}(\frac{N\pi a}{d})\cos(\frac{N\pi z_{N_{\mathrm{V}}}}{d}) & 0 & 0 \\
1 & \cos(\pi z_{N_{\mathrm{V}}+1}/d) & \cos(2\pi z_{N_{\mathrm{V}}+1}/d) & \cdots & \cos(N\pi z_{N_{\mathrm{V}}+1}/d) & 0 & 0 \\
\vdots & \vdots & \vdots & \vdots & \vdots & \vdots & \vdots \\
1 & \cos(\pi z_{N_{\mathrm{VI}}}/d) & \cos(2\pi z_{N_{\mathrm{VI}}}/d) & \cdots & \cos(N\pi z_{N_{\mathrm{VI}}}/d) & 0 & 0 \\
\frac{1}{a\ln(b/a)} & \frac{\pi}{d}f_{1c}(\frac{\pi a}{d})\cos(\frac{\pi z_{N_{\mathrm{VI}}+1}}{d}) & \frac{2\pi}{d}f_{1c}(\frac{2\pi a}{d})\cos(\frac{2\pi z_{N_{\mathrm{VI}}+1}}{d}) & \cdots & \frac{N\pi}{d}f_{1c}(\frac{N\pi a}{d})\cos(\frac{N\pi z_{N_{\mathrm{VI}}+1}}{d}) & 0 & 0 \\
\vdots & \vdots & \vdots & \vdots & \vdots & \vdots & \vdots \\
\frac{1}{a\ln(b/a)} & \frac{\pi}{d}f_{1c}(\frac{\pi a}{d})\cos(\frac{\pi z_{N_{\mathrm{VII}}}}{d}) & \frac{2\pi}{d}f_{1c}(\frac{2\pi a}{d})\cos(\frac{2\pi z_{N_{\mathrm{VII}}}}{d}) & \cdots & \frac{N\pi}{d}f_{1c}(\frac{N\pi a}{d})\cos(\frac{N\pi z_{N_{\mathrm{VII}}}}{d}) & 0 & 0 \\
1 & \cos(\pi z_{N_{\mathrm{VII}}+1}/d) & \cos(2\pi z_{N_{\mathrm{VII}}+1}/d) & \cdots & \cos(N\pi z_{N_{\mathrm{VII}}+1}/d) & 0 & -1 \\
\vdots & \vdots & \vdots & \vdots & \vdots & \vdots & \vdots \\
1 & \cos(\pi z_N/d) & \cos(2\pi z_N/d) & \cdots & \cos(N\pi z_N/d) & 0 & -1 \\
\frac{h_1}{a\ln(b/a)} & f_{1c}(\frac{\pi a}{d})\sin(\frac{\pi h_1}{d}) & f_{1c}(\frac{2\pi a}{d})\sin(\frac{2\pi h_1}{d}) & \cdots & f_{1c}(\frac{N\pi a}{d})\sin(\frac{N\pi h_1}{d}) & 0 & 0 \\
\frac{d-h_4}{a\ln(b/a)} & -f_{1c}(\frac{\pi a}{d})\sin(\frac{\pi h_4}{d}) & -f_{1c}(\frac{2\pi a}{d})\sin(\frac{2\pi h_4}{d}) & \cdots & -f_{1c}(\frac{N\pi a}{d})\sin(\frac{N\pi h_4}{d}) & 0 & 0
\end{bmatrix}
\times
\begin{bmatrix} B_0 \\ B_1 \\ \vdots \\ B_N \\ \phi_{\mathrm{IV}} \\ \phi_{\mathrm{VIII}} \end{bmatrix}
=
\begin{bmatrix} 0 \\ \\ \vdots \\ \\ 0 \\ \phi_0 \\ \vdots \\ \phi_0 \\ 0 \\ \\ \\ \vdots \\ \\ \\ \\ 0 \end{bmatrix}, \tag{26}$$

such that matrix division immediately results in the required vector $[\mathbf{B}] = [\mathbf{A}]^{-1}[\mathbf{C}]$ of unknown coefficients B_0 and B_n from equation (8) as well as ϕ_{IV} and ϕ_{VIII}. Note that the index "N_x" with z in equation (26) stands for the number of discretization points z_i between $z=0$ and the top of the boundary segment denoted by "x" in Figure 1 (e.g., $z_{N\mathrm{IV}}$ is the last discretization point at the top of boundary segment IV, and $z_{N\mathrm{IV}+1}$ is the first one in boundary segment V; also $N_{\mathrm{VIII}} = N$). Appendix A gives further details about the convergence behavior for increasing N and shows that resulting flow field parameters, including F, may be hyperbolically extrapolated to the exact solutions corresponding to $N \to \infty$. Thus, the problem is solved in a novel and direct way without the need for previous conversion of the mixed-type into a single-type boundary value problem.

[25] For the simpler configuration of injection from a push-in probe (i.e., in the absence of open screen intervals above and below the packers), equations (19), (23), (24), and (25) become irrelevant. The system reduces to equations

(20), (21), and (22) with $h_1 = 0$ and $h_4 = d$, which further corresponds to a respective reduction of equation (26). In the opposite case of infinitesimally short packers such that $h_1 = h_2$ and $h_3 = h_4$, all boundary segments along the probe are of the constant head type, and the problem reduces to a single-type boundary value problem. Under this scenario (and known ϕ_{IV} and ϕ_{VIII}) the present trigonometric interpolation approach becomes identical to performing the discrete Fourier (in particular sine or cosine) transform on $\phi(a, z_i)$. The discrete Fourier transform is again known to become identical to the (classic) Fourier decomposition of a continuous periodic function if $N_B \to \infty$. The latter is performed in Appendix B to obtain a fully analytical solution and discussion of the infinitesimally short packer problem.

2.3. Shape Factor *F*

[26] Integrating local radial fluxes $q_{pr} = -\partial\phi/\partial r$ leaving the probe (i.e., for $r = a$), the injection flow rate Q [L^3/T] may be written as

$$Q = -2\pi a K \phi_0 \int_{h_2}^{h_3} \left.\frac{\partial \phi_u}{\partial r}\right|_{r=a} \mathrm{d}z, \tag{27}$$

where $\phi_u = \phi(r, z)/\phi_0$ (dimensionless). By substituting equation (27) into equation (1) a general expression of F is obtained.

$$F = -2\pi a \int_{h_2}^{h_3} \left.\frac{\partial \phi_u}{\partial r}\right|_{r=a} \mathrm{d}z. \tag{28}$$

[27] In the simpler case of injection through a single screen from a push-in probe (or packers extending to top and bottom boundaries) and in the case of using shorter packers between impermeable top and bottom boundaries the integration limits in equation (28) may be set from zero to d, for which the following simplified expressions are found.

[28] Constant head top and bottom boundaries

$$F = 4\pi a \sum_{n=1}^{N} B_{nu} f_1(m_1 a),\ m_1 = (2n - 1)\pi/d, \tag{29}$$

[29] Impermeable top and bottom boundaries

$$F = \frac{2\pi d}{\ln \frac{b}{a}} B_{0u}, \tag{30}$$

[30] Impermeable top and constant head bottom boundary

$$F = 2\pi a \sum_{n=1}^{N} B_{nu} f_1(m_1 a),\ m_1 = (2n - 1)\pi/(2d), \tag{31}$$

where $B_{0u} = B_0/\phi_0$ and $B_{nu} = B_n/\phi_0$, i.e., dimensionless coefficients for unit injection head. As above, f_1 in equations (29) and (31) is chosen from equations (11) and (12) to honor a constant head or impermeable lateral boundary, respectively. Interesting to note is that equation (30) only depends on B_{0u}, which by inspecting equation (8) with $r = a$ in a Fourier series context, is seen to represent the mean head along the device (for unit ϕ_0). In other words, B_0 is the head required at a fully screened probe to inject an equal flow rate Q as from a partially screened probe using an injection head ϕ_0. Also, for a fully screened probe, B_n for $n > 0$ in equation (8) become zero, and the solution correctly collapses to radial flow toward a fully penetrating well in a confined aquifer with a constant head outer boundary. Equation (30) further reflects that b/a needs to be finite in order to achieve flow (i.e., $F > 0$) for a finite injection head if both top and bottom boundaries are impermeable.

3. Results and Validation

[31] For the example configuration of equations (19)–(25) (and $N_B = 1280$), Figure 2 depicts resulting dimensionless head ϕ_p/a and dimensionless radial flux q_{pr}/K distributions along a fully screened well with injection between two packers. Solid lines correspond to the case of both top and bottom boundaries impermeable, while dashed lines are for constant head top and bottom boundaries; the lateral boundary is constant head in both cases. Compliance with prescribed constant head and no flow boundary conditions over their respective intervals may be easily verified in both cases along with the fact that ϕ_p is constant but larger than zero in the open screen intervals beyond the packers if the adjacent boundaries are impermeable. Furthermore, Figure 2b suggests (in agreement with Figure A1) that local fluxes at the transitions between constant head and impermeable boundary segments along the probe or well become locally very large or infinite. Finally, it may be correctly observed that flow along the open screen intervals is negative (i.e., inward) if top and bottom boundaries are constant head (dashed line), while the direction of flow along the open screen intervals is inward and then outward for impermeable top and bottom boundaries (solid line) to meet the condition of zero total inflow and outflow over those segments as imposed by equations (24) and (25). Figure 3 further illustrates and validates solutions by showing contour plots of $\phi(r, z)$ for different internal and external boundary conditions. Figures 3a and 3b correspond to the solid and dashed lines of Figure 2, respectively. Compliance with external boundary conditions is verified by observing constant head lines approaching impermeable boundaries perpendicularly and by constant head lines becoming parallel to constant head boundaries in their vicinity. Figures 3c and 3d represent two cases of injection from a probe (i.e., packers extend to top and bottom boundaries) where the lateral boundaries are impermeable (e.g., as in laboratory barrel experiments). In Figure 3c both top and bottom are constant head, while in Figure 3d, only the top is constant head and the bottom impermeable.

3.1. Injection From a Probe (Field Conditions)

[32] As shown in Figure A1 of Appendix A, the convergence behavior of F with increasing N is of the same hyperbolic type as with other flow field parameters and may, hence, be conveniently extrapolated to exact solutions for $N \to \infty$. For an error margin of 1% in extrapolated F values, Figure 4 summarizes the resulting shape factors from equations (29), (30), and (31) for injection from a probe with $h_1 = 0$ and $h_4 = d$ in Figure 1 as a function of s/a

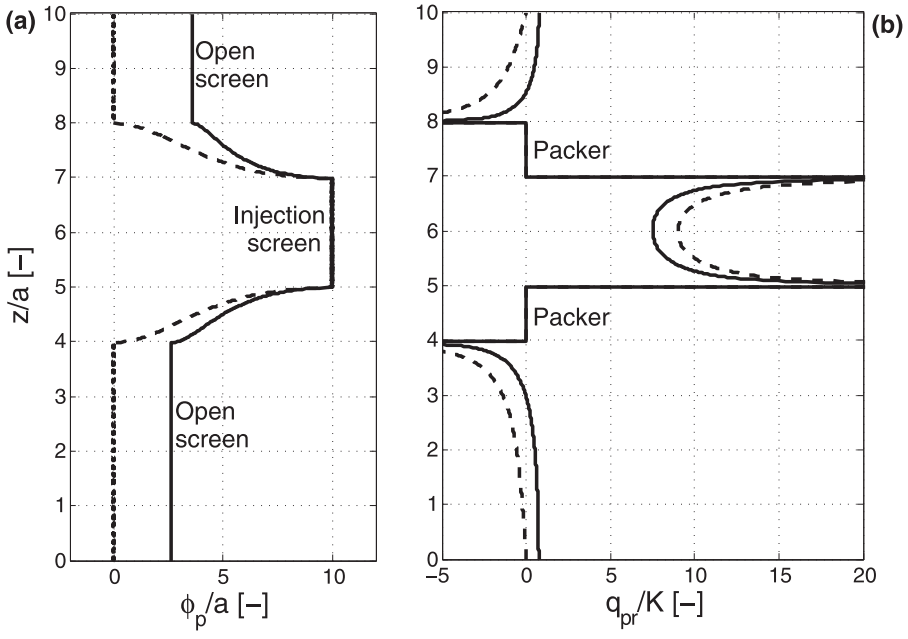

Figure 2. (a) Hydraulic head ϕ_p / a and (b) radial flux q_{pr}/K distributions along fully screened well for injection between two packers. Solid lines are for the example configuration of Appendix A where top and bottom boundaries are impermeable. Dashed lines are for the same configuration but with constant head top and bottom boundaries.

(where $s = h_3 - h_2$ [L] is the length of the injection screen vertically centered between boundaries), d/s, and different top and bottom boundary types (thick solid line, constant head top and bottom; thin solid line, impermeable top and bottom; dashed line, constant head top and impermeable bottom or vice versa). Typical for field conditions, the constant head lateral boundary is located at $b/a = 1000$, which is large enough to not affect the outcome if at least one of top and bottom boundaries is constant head. In case both top and bottom boundaries are impermeable, as stated above, a finite value of b/a is required for $F > 0$. As to be expected, for a given geometric configuration, i.e., s/a and d/s, F/a is always largest if both top and bottom are constant head and smallest if both are impermeable. For increasing values of d/s, however, it is seen that the types of top and bottom boundaries have a decreasing effect on F/a, i.e., the three curves for a given value of s/a converge to a shape factor, whose value increases with s/a and which corresponds to an infinite flow domain, where the types and distances of top and bottom boundaries do not matter anymore. On the other hand, for small values of d/s approaching 1 such that top and bottom boundaries approach the injection screen extremes, F/a approaches infinity if at least one of the boundaries is constant head (flow short-circuiting; see Appendix B). If both boundaries are impermeable, then F approaches a minimum equal to $2\pi d / \ln(b/a)$, which corresponds to the case of a fully penetrating well in a confined aquifer.

[33] While Figure 4 is limited to injection screens vertically centered between top and bottom boundaries, Figure 5 displays F/a for different values of screen length s/a and distance h_1/s to a single nearby boundary. In Figure 5, $d/s = 50$ is set to be large enough for the distant boundary to not have a significant impact on results (compare Figure 4), and the lateral boundary is located at infinity. Thick lines correspond to the injection screen approaching a constant head boundary, while thin lines are for nearby impermeable boundaries. It is seen that for large values of h_1/s, values of F/a agree with those from Figure 4 for large values of d/s; as h_1 decreases, the screen approaches one of the boundaries. As to be expected, if the approached boundary is constant head, the thick lines indicate that F/a increases (up to a theoretically infinite value for $h_1 = 0$; see Appendix B), and if the boundary is impermeable, then F/a decreases to a minimum value. In general, it may be observed from Figure 5 that the proximity of the injection screen to an impermeable or constant head boundary does not significantly affect F by more than an absolute value of $\pm a$ as long as $h_1/s > 5$. By multiplying the abscissa by s/a of each line, F/a is obtained as a function of h_1/a. The double arrows in Figure 5 are located at $h_1/a = 20$, which appears to be the limit, below which the relative impact on F because of a nearby boundary exceeds approximately 5%. As conductivity measurements may vary over several orders of magnitude, the latter interpretation in terms of h_1/a seems to be more useful in practice.

[34] For the absence of any nearby boundaries, Figure 6 gives a graphical validation of the present approach against previous ones defined by *Hvorslev* [1951] (spheroidal approximation),

$$F = \frac{2\pi s}{\ln\left[\frac{s}{2a} + \sqrt{1 + \left(\frac{s}{2a}\right)^2}\right]} = \frac{2\pi s}{a \sinh\left(\frac{2}{sa}\right)}, \tag{32}$$

by the American Society for Testing and Materials (ASTM) [*Chapuis and Chenaf*, 2003] (equal surface area spherical approximation),

$$F = 2\pi\sqrt{2sa} \approx 8.9\sqrt{sa}, \tag{33}$$

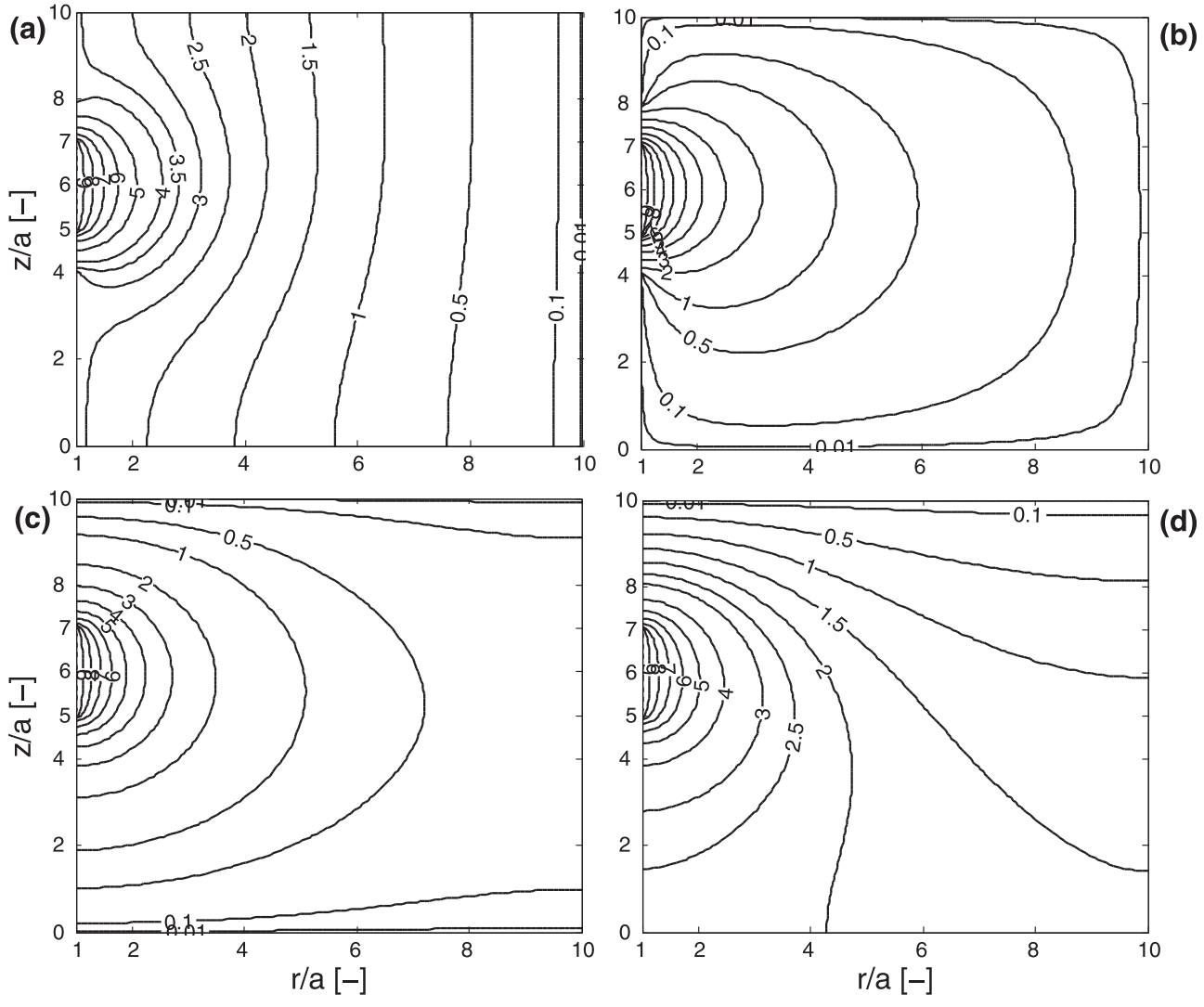

Figure 3. Solutions of $\phi(r, z)$ for $\phi_0/a = b/a = d/a = 10$ and (a) injection between double packers with impermeable top and bottom and constant head lateral boundaries, (b) injection between double packers with constant head top, bottom, and lateral boundaries, (c) injection from probe with constant head top and bottom and impermeable lateral boundaries, and (d) injection from probe with constant head top and impermeable bottom and lateral boundaries.

and by *Ratnam et al.* [2001] (finite element plus curve fitting),

$$F = 0.5691s + 7.4144\sqrt{sa}\,. \tag{34}$$

[35] For *Mathias and Butler*'s [2007] full semianalytical approach as well as *Rehbinder*'s [2005] long packer approximation, no simple expressions are available. Figure 6 illustrates that the ASTM formula is in good agreement down to $s/a \approx 1$, while Hvorslev's formula begins to significantly overestimate F/a below $s/a \approx 2$. The latter is a known shortcoming and is discussed by *Mathias and Butler* [2006], who offer an improvement for Hvorslev's formula for $s/a < 2$. Equation (33) is based on a spherical equal surface approximation of the screen and, hence, becomes increasingly inaccurate as s/a grows. While equations (32) and (33) are based on geometrical simplifications, the other approximations try to honor the exact geometry of the boundaries and rely on more complex mathematical approximations. The agreement of the results of *Ratnam et al.* [2001] and *Rehbinder* [2005] (thin black line) with the present results is seen to be good over the entire range depicted. Excellent agreement (with, in fact, indistinguishable lines in Figure 6; thick black line) is achieved with the results of *Mathias and Butler* [2007]. Yet another independent validation of the present method may be obtained by comparison with results from a large numerical model for a direct-push permeameter of *Liu et al.* [2008], who report hydraulic heads at two locations along a probe for injection from a short screen. Agreement is good (within 5% of injection head) when assuming impermeable top and bottom boundaries and even better (within 0.5% of injection head) when assuming constant head top and bottom.

3.2. Injection From a Probe (Laboratory Conditions)

[36] Calibration of injection probes under field conditions is problematic, as true values of hydraulic conductivity are

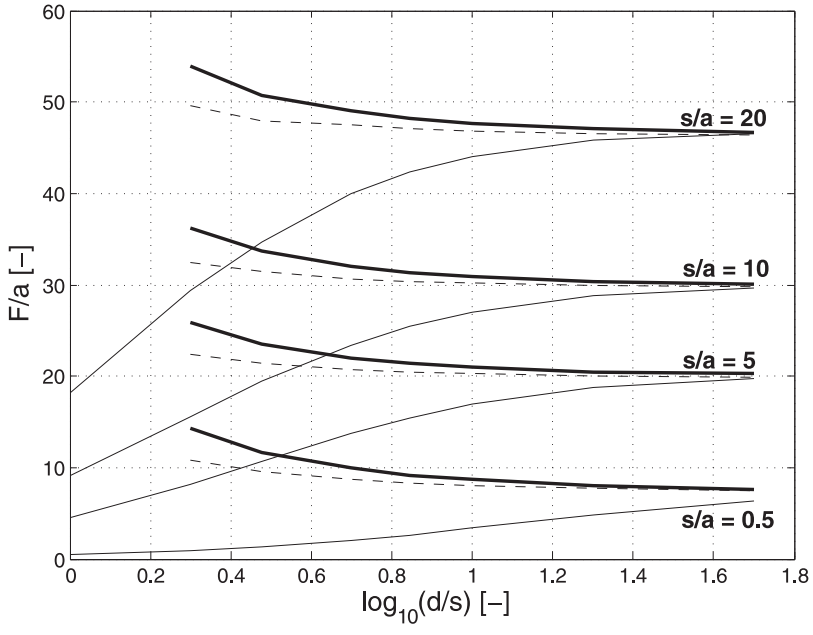

Figure 4. F/a for injection from vertically centered single-screen probe (no open screen intervals except for injection screen) as a function of s/a and $\log_{10}(d/s)$ and for different top and bottom boundary conditions (constant head lateral boundary at $b/a = 1000$). Thick solid line, constant head top and bottom; thin solid line, impermeable top and bottom; dashed line, constant head top and impermeable bottom (or vice versa).

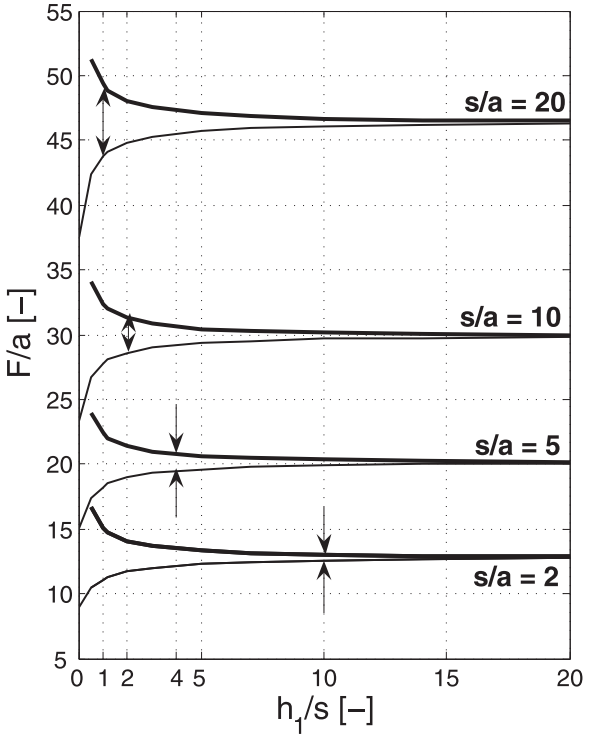

Figure 5. F/a for injection from noncentered single-screen probe (no open screen intervals except for injection screen) as a function of s/a and distance to boundary h_1/s ($d/s = 50$ and lateral boundary at infinity). Thick solid line, approaching constant head boundary; thin solid line, approaching impermeable boundary. Double arrows indicate locations of $h_1/a = 20$.

generally not available. Laboratory barrel experiments are convenient because the entire barrel packed with test material above a bottom gravel pack may be used as a column in a constant or falling head conductivity experiment for obtaining independent and relatively reliable measurements of K. Figure 7 depicts F/a for different screen and barrel geometries (s/a, d/a, and b/a) as well as boundary conditions at the barrel bottom (gravel pack or not). The top boundary is always constant head (i.e., water level above test material), while the barrel wall represents an impermeable boundary. The thick black line is the same as in Figure 6 and corresponds to a field situation where external boundaries do not have a significant impact. For the remaining lines, two lines with a particular color and pattern are given to correspond to the same boundary and barrel geometries (see legend). The top line of each pair of lines corresponds to a constant head bottom boundary, while the bottom one corresponds to an impermeable bottom. Obviously, the particular barrel geometry and type of bottom boundary condition significantly affect F, and hence, they need to be accounted for explicitly in the test interpretation. However, it is interesting to note that barrels of $d/b = 1$ with impermeable bottoms (bottom blue lines) as well as barrels of $d/b = 2$ with constant head bottoms (top green lines) lead to shape factors very close to field conditions in the absence of nearby boundaries (black line). For $b/a > 25$ this holds with high accuracy for $s/a < 10$ and up to an approximate error of 10% for $s/a < 20$. Thus, designing a barrel test of known K_{lab} such that its shape factor is equal to F under field conditions allows for an extremely simple injection test interpretation as $K_{\text{field}} = K_{\text{lab}} Q_{\text{field}} \phi_{0\text{lab}} / (Q_{\text{lab}} \phi_{0\text{field}})$. This avoids dealing with probe specific shape factors in laboratory and field practice.

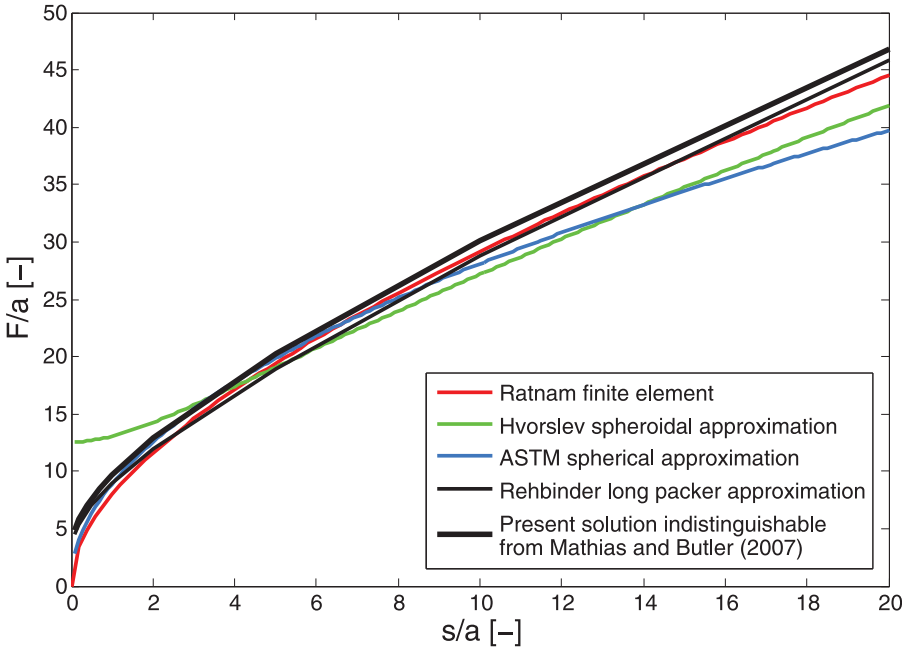

Figure 6. F/a from different approaches for injection from probe and different injection screen geometries. All boundaries are constant head and distant with $d/s = 50$ and $b/a >> 1$.

3.3. Injection Using Single or Double Packers

[37] The solid lines in Figure 8 summarize shape factors F/a from the present solutions for cases of injection from a screen interval of length s delimited by two impermeable packers of finite (and equal) length p with open screen intervals above and below the packers. While F/a is a function of b/a even if $b/a >> 1$ when both top and bottom boundaries are impermeable, Figure 8 considers all boundaries constant head with $b/a >> 1$ and $d/s = 50$, i.e., far away from the screen. Shorter packers (smaller p/s), as expected, increase F/a in an approximately constant manner, which indicates that changes in packer length only affect the flow fields in the vicinity of the screen ends, thus being essentially independent of s/a unless s/a is very small. It is interesting to note for practice that above $p/s \approx 1$, F is only slightly affected by the finite length of the packers; especially for $s/a > 5$, the difference in F to longer packers is consistently smaller than approximately a. By multiplying the values of p/s in Figure 8 with s/a from the abscissa, lines of F/a over s/a for constant values of p/a are obtained. The circles and squares represent points on such lines for $p/a = 1$ and 4, respectively. Similar to Figure 5, it may be observed that the influence of packer length on F may be more conveniently expressed in relative terms using p/a instead of the perhaps more intuitive first choice p/s. In particular, it can be inferred from the circles and squares in Figure 8 that $p/a = 1$ and 4, for example, correspond to increases in F by approximately 20% and 10%, respectively, with respect to $p >> a$. The influence of nearby top or bottom boundaries on double-packer injection tests depends on a series of parameters (s/a, p/a, h_1/a, and type of boundary approached) and is best evaluated individually for a given test configuration (i.e., s/a and/or p/a). For injection between a packer and an impermeable bottom layer (single packer test), F/a may also be found from Figure 8 by entering the chart with $p/(2s)$ instead of p/s and $2s/a$ instead of s/a and then halving the respective outcome for F/a. This is a consequence of the fact that the flow field for a single-packer injection test corresponds exactly to one half of the flow field of a double-packer injection test.

[38] Figure 8 is also valuable for the situation of injection from a probe if p is taken to represent the impermeable probe tip length under the injection screen. For this case, a lower bound for F/a is found by assuming that the inner boundaries above and below these fictitious packers are impermeable, while an upper bound for F/a is found by assuming that the inner boundaries above and below the fictitious packers are constant head, i.e., infinitely conductive. In reality, the inner boundary above the top packer is impermeable (probe casing), and below the bottom packer (i.e., below the probe tip) is the transition to a cylinder of some finite conductivity. From this, it may be concluded that errors in F because of the conceptual assumption of a long probe tip beneath the injection screen become less than a for $p/s \geq 1$ (given $s/a \geq 5$) or less than 10% for $p/a \geq 4$.

[39] The scenario of double-packer injection with distant boundaries is also considered by *Mathias and Butler* [2007] and by *Rehbinder* [1996] for a short-packer approach, and their results are used for additional validation of the present results in Figure 8. While Rehbinder's short-packer solution (shown as dashed lines for $p/s = 0.05$ and 1) presents moderate agreement, the results of *Mathias and Butler* [2007] are again indistinguishable from the present ones. However, as shown in Appendix B, *Mathias and Butler*'s [2007] result for infinitesimally short packers contains an unsatisfactorily divergent infinite series. The 10,000 terms

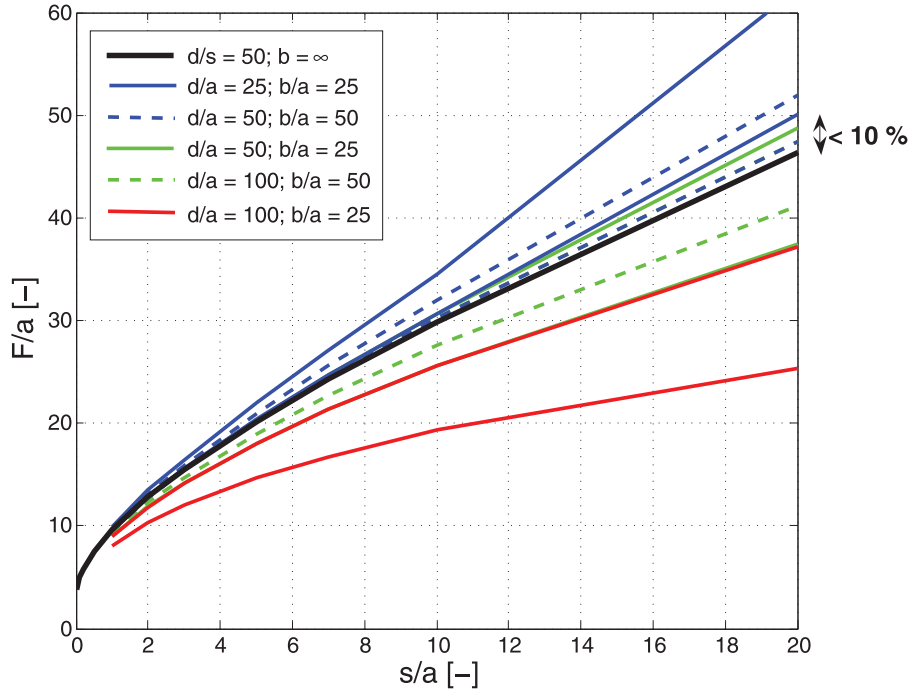

Figure 7. F/a for injection in laboratory barrel setups of different geometries s/a, d/a, and b/a as well as different bottom boundary types. Top and lateral boundaries are always constant head and impermeable, respectively. For each line pattern and color, there are two lines; the top line is for constant head bottom boundary (e.g., gravel pack hydraulically connected to constant head upper boundary), and the bottom line is for impermeable bottom boundary (no gravel pack). The bottom dashed blue and top dashed green lines are practically indistinguishable, which is also true for the bottom solid green and top solid red lines.

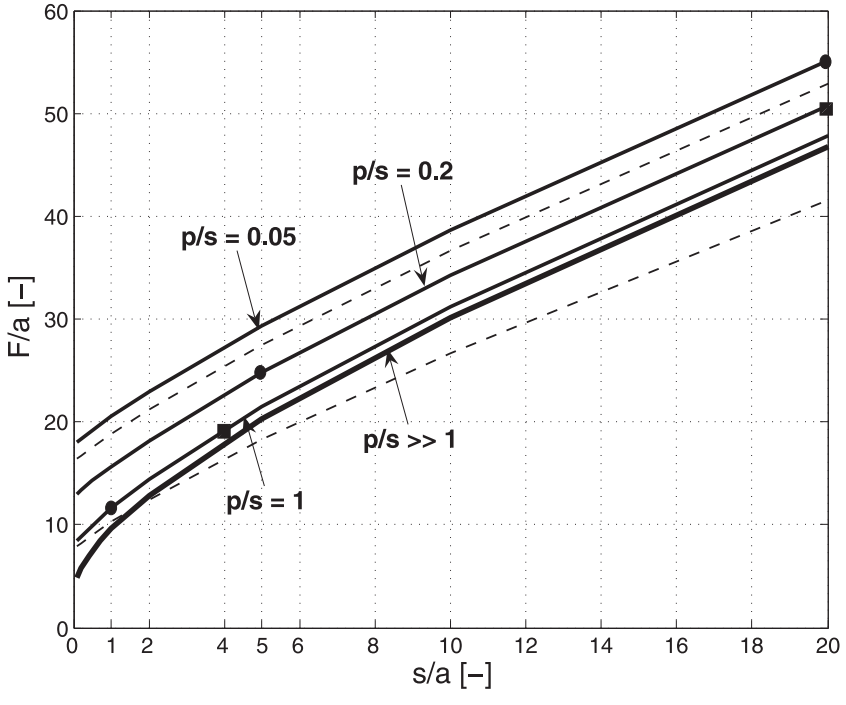

Figure 8. F/a for different injection screen (s/a) and packer (p/s) geometries from the present approach with all boundaries constant head and distant at $d/s = 50$ and $b/a >> 1$ (solid lines; indistinguishable from the full solution of *Mathias and Butler* [2007]). Dashed lines are *Rehbinder*'s [1996] short-packer approximation for $p/s = 0.05$ and 1. Circles indicate locations of $p/a = 1$, and squares indicate $p/a = 4$.

used to approximate the infinite series in their equations (21) and (31) are insufficient to achieve convergence for very small values of p/s. However, the regression relationship given in their equation (40) accurately approximates the case when $p/s = 0.005$ and should be assumed for $p/s = 0.005$ (as opposed to $p/s = 0$, which is what is currently stated in their paper). Fortunately, this does not impair the validity and relevance of *Mathias and Butler*'s [2007] results for all practical purposes.

3.4. Anisotropic Conductivity

[40] In practice it is common to encounter situations where hydraulic conductivity in the horizontal direction K_r [L/T] is significantly different (e.g., several orders of magnitude larger) than its vertical counterpart K_z [L/T]. Given the respective anisotropy ratio $\rho^2 = K_z/K_r$ (dimensionless), a scaling of the horizontal coordinate to $r' = r\rho$ while maintaining $z' = z$ allows for treating the resulting flow domain as isotropic with conductivity K_r (such that continuity of flows after scaling is assured [*Hvorslev*, 1951]). Thus, the present approach remains generally valid if hydraulic conductivity is axially anisotropic with the principal anisotropy axes being horizontal and vertical. In particular, results for F/a reported above remain directly applicable if $a' = a\rho$ is used instead of a such that equation (1) estimates K_r to subsequently obtain $K_z = \rho^2 K_r$. However, ρ is generally not known before hand and needs to be assumed or measured independently.

4. Summary

[41] Subsurface hydraulic conductivity K is a fundamental hydrogeological parameter whose in situ measurement is generally performed through injection tests from screened probes or well screen intervals delimited by impermeable packers. While K is directly proportional to an observed ratio of injection flow rate Q to injection head ϕ_0, it is also proportional to the shape factor F, which is determined by the geometry of the injection flow field and, hence, the geometry of the injection device (internal boundary conditions) as well as the flow domain (external boundary conditions). For the purpose of evaluating F over a wide range of scenarios, the present work presents general solutions to the axisymmetric steady state flow problem for arbitrary combinations of external boundary types and distances. The internal boundary may consist of an arbitrary number of impermeable and constant head intervals. The resulting mixed-type boundary value problem is solved directly in a novel and relatively simple way using a trigonometric interpolation approach. This avoids previous conversion into a single boundary type problem as required with recent alternative approaches and allows for a simple (hyperbolic) extrapolation from approximate to exact results. Through an adequate scaling of the radial coordinate the approach becomes generally valid for flow domains with anisotropic conductivity, where K is different between the vertical and horizontal directions.

[42] A series of dimensionless charts is given to allow for a quick determination of F for different injection screen geometries s/a under a range of scenarios: (1) injection from a probe (or using long double packers) centered between different combinations of impermeable and constant head top and bottom boundaries at different distances, (2) injection from a probe (or using long double packers) near a single impermeable or constant head boundary, (3) injection in laboratory barrel experiments with all boundaries nearby, the lateral being impermeable, and (4) injection between double packers of different lengths and distant external boundaries. Interesting findings include F being affected by less than 5% if a minimum distance of approximately 10 times the probe diameter is maintained to an impermeable or constant head horizontal boundary (Figure 5). Similarly, using a minimum packer length of twice the well diameter does not affect F by more than 10% compared to longer packers; the latter also applies to the length of impermeable tips of push-in probes below the screen. For injection tests in sand barrels (e.g., for probe calibration) it is found that shape factors within 10% of those of field situations (in the absence of nearby boundaries) may be created by using $d/b = 1$ for impermeable barrel bottoms and $d/b = 2$ if a gravel pack at the barrel bottom is deployed to establish a constant head boundary (with water freely draining out of barrel).

[43] Comparison and validation of results is performed against a number of existing approximate, semianalytical, and numerical approaches available for scenarios where the influence of external boundaries is negligible. Notably, respective shape factors of the present approach are identical to those obtained by the method of *Mathias and Butler* [2007]. However, for extreme cases of very short packers, *Mathias and Butler*'s [2007] solution was found to be incomplete. We present a respective correction in the form of a fully analytical solution for the limit of infinitesimally short packers (see Appendix B).

Appendix A: Convergence Behavior

[44] For the wide range of boundary configurations investigated, it was observed that the B_n coefficients always converge to zero as n increases and that particular flow field parameters (e.g., F or local heads and fluxes) converge hyperbolically toward a stable value for $N_B \to \infty$ (such hyperbolic convergence is also observed by *Boast and Kirkham* [1971]). Figure A1 represents examples of the latter for arbitrarily chosen $b/a = d/a = \phi_0/a = 10$, $h_1/a = 4$, $h_2/a = 5$, $h_3/a = 7$, and $h_4/a = 8$, i.e., for injection from a screen of length $2a$ delimited by two packers of length a, which are asymmetrically located in a stratum between two confining layers. Depicted as functions of $1/N_B$ are the relative heads ϕ/a (dashed lines) and relative fluxes q/K (dot-dashed lines) for $z/a = 4.5$, 6, and 8 (indicated in the indices), i.e., for the center of the bottom packer, the center of injection interval, and the top extreme of top packer, respectively. N_B is increased from an initial value of 10 through consecutive multiplication by 2 until 1280 (circles). It is observed that all ϕ/a and q/K approach a relatively straight line toward the left when plotted over $1/N_B$. This allows for simple linear extrapolation of two consecutive data points onto $1/N_B = 0$, i.e., the exact solutions for $N_B \to \infty$, and a sufficiently large value of N_B is reached when two consecutive extrapolated values are within a prescribed margin. An exception to this is q_s/K, which provides some evidence that flow is singular (infinite flux) at the transitions between impermeable and constant head boundaries along the well or probe. As infinite fluxes

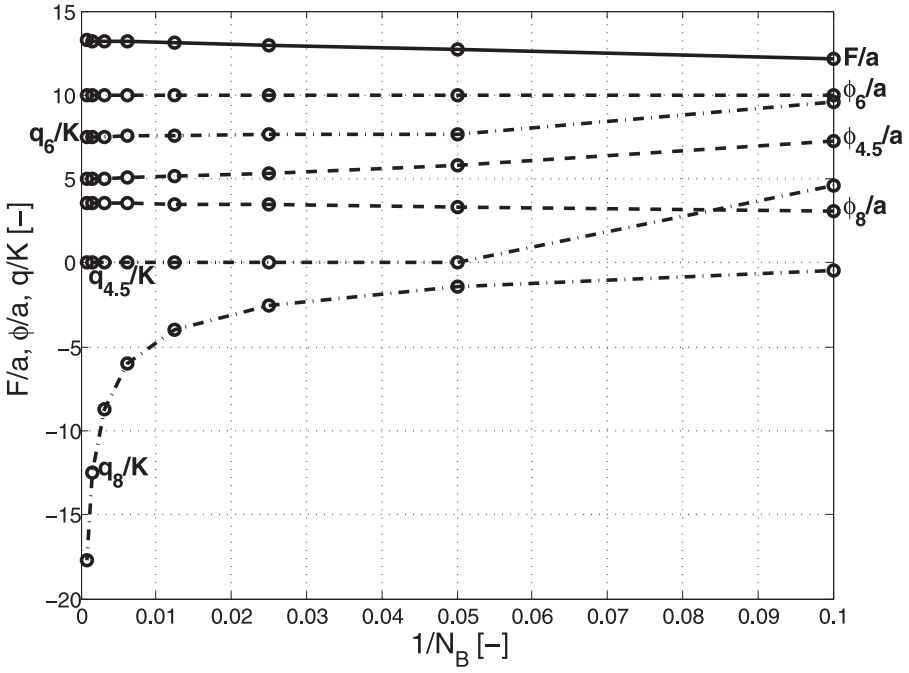

Figure A1. Hyperbolic convergence of F/a, ϕ/a, and q/K with N_B for injection using double packers between two confining layers, where indices indicate locations $z/a = 4.5$, 6, and 8 along the well. Here $b/a = d/a = \phi_0/a = 10$, $h_1/a = 4$, $h_2/a = 5$, $h_3/a = 7$, and $h_4/a = 8$.

are physically impossible, the governing equation (equation (3)) of the present approach appears to be invalid near the extremes of well casings and packers. However, F converges to a finite value, indicating that injection flow does remain finite (integrable). Successful validation of F against independent (e.g., numerical) methods, which do not produce these flow singularities, demonstrates that equation (3) is, indeed, physically valid everywhere else (i.e., at all nonsingular locations) in the flow domain. Although not a necessary requirement, maximum convergence with N_B is achieved if the screen and packer limits coincide with discretization interval limits and if average values over discretization intervals are used for any location inside a respective interval. An attempt to lower required N_B by enlarging interval spacing distant from the screen and packers (as done by *Mathias and Butler* [2007]) leads into the context of trigonometric interpolation for unevenly spaced data and was not further pursued as computational time was found not to act as a limiting factor.

Appendix B: Analytical Solution for Infinitesimally Short Packers

[45] If $h_1 = h_2$ and $h_3 = h_4$ in Figure 1, the impermeable packers become infinitesimally short, and the internal boundary conditions are all of the constant head type, which is a significant simplification with respect to the general mixed boundary problem. A fully analytical solution is found for this case and provides some interesting theoretical insight on whether total injection flow becomes infinite or not, a topic which *Rehbinder* [1996] and *Mathias and Butler* [2007] are in disagreement about. For the sake of concurrence with these previous studies, consider constant head top, bottom, and lateral boundaries, such that equations (7) and (10) apply. Equation (10) is identical to 1 for $r = a$ (i.e., along the well surface), and if $N \to \infty$, the coefficients B_n in equation (7) become the coefficients of a sine-Fourier series of the known head distribution along the well ($\phi(a, z) = 0$ for $0 \le z \le h_2$ and $h_3 \le z \le d$; $\phi(a, z) = \phi_0$ for $h_2 \le z \le h_3$), which may be found as

$$B_n = \frac{2\phi_0}{n\pi}[\cos(m_1 h_2) - \cos(m_1 h_3)],\ m_1 = n\pi/d\,, \qquad \text{(B1)}$$

such that the analytical solution of the problem is complete. By using equation (28) a general expression of F is obtained as

$$F = 4a\sum_{n=1}^{\infty}\frac{f_{1c}(m_1 a)}{n}[\cos(m_1 h_2) - \cos(m_1 h_3)]^2\,. \qquad \text{(B2)}$$

[46] From equation (11) it may be seen that $f_{1c}(m_1 a)$ converges to 1 as n increases and the squared term in brackets is always positive. This and the fact that $\sum_{n=1}^{\infty}\frac{1}{n} \to \infty$ is sufficient to prove that equation (B2) does not converge; that is, F and, hence, Q are infinitely large in the case of infinitesimally short packers (the only exception to this is the case of $h_2 = h_3$, i.e., when the injection screen interval itself becomes infinitesimally short). Clearly, infinitesimally short packers and infinite injection flows are beyond physical reality; however, the result bears some significance in that practitioners are warned from arbitrarily minimizing packer sizes as, depending on particular site conditions, the governing equation (3) based on Darcy flow may not hold over significant portions of the flow domain near the short packers. These conclusions are also applicable to injection screens immediately next to a top or bottom constant head

boundary where the geometric distance (flow paths) between source (screen) and sink (boundary) is even shorter. Note, however, that flow singularities discussed in Appendix A do not share the property of causing F and Q to be infinite.

[47] In contrast, if both top and bottom boundaries are impermeable, equation (30) dictates that F has to be finite at steady state even for infinitesimally short packers since B_{0u} was found to be the (naturally finite) mean head along the well. Also, the same flow entering the open screen intervals needs to leave them again and reenter the aquifer flow field until meeting the lateral constant head boundary. Using a similar procedure as in equations (B1) and (B2) for constant head top and bottom boundaries, it may be shown that the head difference between the injection screen and the open screen intervals above and below the infinitesimally short packers becomes infinitesimally small, such that the whole well behaves as if injection was uniformly applied along all of it (no packers present). For a given set of parameters a, b, and d the shape factor F is then a maximum, independent of s.

[48] **Acknowledgments.** The first author would like to thank the Austrian Science Fund (FWF) for an Erwin-Schrödinger Fellowship (project number J2677-N14) to perform this work. Further funding was provided by the Environmental Remediation Science Program (ERSP), the U.S. Department of Energy (grant number DE-FG02-08ER64585), and the U.S. Department of Defense (project number ER0831) under the Environmental Security Technology Compliance Program (ESTCP).

References

Boast, C. W., and D. Kirkham (1971), Auger hole seepage theory, *Soil Sci. Soc. Am. Proc.*, *35* (3), 365–373.

Butler, A. P., S. A. Mathias, A. J. Gallagher, D. W. Peach, and A. T. Williams (2009), Analysis of flow processes in fractured chalk under pumped and ambient conditions, *Hydrogeol. J.*, *17*, 1849–1858, doi:10.1007/s10040-009-0477-4.

Butler, J. J., P. Dietrich, V. Wittig, and T. Christy (2007), Characterizing hydraulic conductivity with the direct-push permeameter, *Ground Water*, *45*, 409–419, doi:10.1111/j.1745-6584.2007.00300.x.

Chang, C. C., and C. S. Chen (2002), An integral transform approach for a mixed boundary problem involving a flowing partially penetrating well with infinitesimal well skin, *Water Resour. Res.*, *38*(6), 1071, doi:10.1029/2001WR001091.

Chang, C. C., and C. S. Chen (2003), A flowing partially penetrating well in a finite-thickness aquifer: A mixed-type initial boundary value problem, *J. Hydrol.*, *271*, 101–118, doi:10.1016/S0022-1694(02)00323-2.

Chapuis, R. P., and D. Chenaf (2003), Variable-head field permeability tests in driven flush-joint casings: Physical and numerical modeling, *Geotech. Testing J.*, *26*(3), 1–12.

Dietrich, P., J. J. Butler, and K. Faiß (2008), A rapid method for hydraulic profiling in unconsolidated formations, *Ground Water*, *46*, 323–328, doi:10.1111/j.1745-6584.2007.00377.x.

Dwight, H. B. (1947), *Tables of Integrals and Other Mathematical Data*, Macmillan, New York.

Hinsby, K., P. L. Bjerg, L. J. Andersen, B. Skov, and E. V. Clausen (1992), A mini slug test method for determination of a local hydraulic conductivity of an unconfined sandy aquifer, *J. Hydrol.*, *136*, 87–106.

Hvorslev, M. J. (1951), Time lag and soil permeability in groundwater observations, *Bull. U.S. Army Corps of Eng. Waterw. Exp. Stn.*, *36*.

Kirkham, D. (1959), Exact theory of flow into a partially penetrating well, *J. Geophys. Res.*, *64*(9), 1317–1327.

Liu, G., G. C. Bohling, and J. J. Butler (2008), Simulation assessment of the direct-push permeameter for characterizing vertical variations in hydraulic conductivity, *Water Resour. Res.*, *44*, W02432, doi:10.1029/2007WR006078.

Mathias, S. A., and A. P. Butler (2006), An improvement on Hvorslev's shape factors, *Geotechnique*, *56*(10), 705–706, doi:10.1680/geot.2006.56.10.705.

Mathias, S. A., and A. P. Butler (2007), Shape factors for constant-head double-packer permeameters, *Water Resour. Res.*, *43*, W06430, doi:10.1029/2006WR005279.

Perina, T., and T. C. Lee (2006), General well function for pumping from a confined, leaky or unconfined aquifer, *J. Hydrol.*, *317*, 239–260, doi:10.1016/j.jhydrol.2005.05.020.

Peursem, D. V., V. Zlotnik, and G. Ledder (1999), Groundwater flow near vertical recirculatory wells: Effect of skin on flow geometry and travel times with implications for aquifer remediation, *J. Hydrol.*, *222*, 109–122.

Price, M., and A. T. Williams (1993), A pumped double-packer system for use in aquifer evaluation and groundwater sampling, *Proc. ICE, 2*, *101*, 85–92.

Ratnam, S., K. Soga, and R. W. Whittle (2001), Revisiting Hvorslev's intake factors using the finite element method, *Geotechnique*, *51*(7), 641–645.

Rehbinder, G. (1996), The double packer permeameter with narrow packers: Analytical solution for non-steady flow, *Appl. Sci. Res.*, *56*(4), 255–279.

Rehbinder, G. (2005), Relation between non-steady supply pressure and flux for a double packer permeameter: An approximate analytical solution, *Flow Turbul. Combust.*, *74*, 1–20, doi:10.1007/s10494-005-2757-y.

Sedighi, A., H. Klammler, C. Brown, and K. Hatfield (2006), A semi-analytical model for predicting water quality from aquifer storage and recovery system, *J. Hydrol.*, *329*, 403–412, doi:10.1016/j.jhydrol.2006.02.035.

Sneddon, I. N. (1966), *Mixed Boundary Value Problems in Potential Theory*, North-Holland, Amsterdam.

Sudicky, E. A. (1986), A natural gradient experiment on solute transport in a sand aquifer: Spatial variability of hydraulic conductivity and its role in the dispersion process, *Water Resour. Res.*, *22*(13), 2069–2092.

Weight, W. D., and J. L. Sonderegger (2001), *Manual of Applied Field Hydrogeology*, McGraw-Hill, New York.

Zaslavsky, D., and D. Kirkham (1964), The streamline function for axially symmetric groundwater movement, *Soil Sci. Soc. Am. Proc.*, *28*, 156–160.

Zlotnik, V., and G. Ledder (1996), Theory of dipole flow in uniform anisotropic aquifers, *Water Resour. Res.*, *32*(4), 1119–1128.

K. Hatfield, H. Klammler, and B. Nemer, Department of Civil and Coastal Engineering, University of Florida, 365 Weil Hall, PO Box 116580, Gainesville, FL 32611, USA. (haki@gmx.at)

S. A. Mathias, Department of Earth Sciences, Durham University, Durham DH1 3HP, UK.